LASER & PHOTONICS REVIEWS
www.lpr-journal.org

Polarization Steering Light Beam Shifts via a High-Efficiency Photonic Crystal Slab

Shunben Wu, Xinhao Wang, Xingqi Zhao, Lixi Rao, Wenzhe Liu, Jiajun Wang, Lei Shi,* and Jian Zi*

The manipulation of light fields using micro/nano photonic structures has become a pivotal area in modern optics, enabling precise control over light propagation and interaction at subwavelength scales. This study demonstrates a high-efficiency method for steering light beam displacement at optical interfaces through polarization control using a reflective photonic crystal (PhC) slab. The reflective PhC slab enhances cross-polarization efficiency by reducing scattering channels, facilitating clear observation of beam shifts without the need for additional polarization analysis. By varying the polarization state of incident light, continuous magnitude and direction control over the beam shift at the PhC slab are achieved. In practical experiments, a maximum cross-polarized efficiency over 74% and the tunable displacement range reaching up to 14 wavelengths at 780 nm are realized. This work proposes an effective approach to realizing controllable beam displacement, while also inspiring future developments in precise and efficient beam steering through photonic band and polarization engineering.

1. Introduction

Light field manipulation based on micro/nano photonic structures has emerged as a cornerstone in modern optics, offering unprecedented capabilities in controlling light propagation, emission, and interaction at subwavelength scales.[1–3] As periodically arrayed nanostructures, photonic crystal (PhC) slabs stand out as a representative example of these photonic structures, and have proven to be effective tools for multi-dimensional light manipulations. Recently, PhC slabs are explored to carry novel polarization degrees of freedom in photonic bands, forming topological polarization configurations in momentum space involving various polarization singularities like bound states in the continuum and circularly polarized points.[4–10] These inherent topological polarization configurations can interact with light fields in free space, enabling a variety of novel optical effects and applications,[11–14] such as vortex beam generation,[15,16] photonic Hall effect,[17,18] optical chirality control,[19–23] lasing,[24] polarization-dependent nonlinear enhancement,[25–27] and so on.[28] Moreover, the periodicity in real space and hidden frequency dimensions in photonic bands make PhC slabs versatile platforms for developing compact, alignment-free photonic devices in light manipulations.

Among the various topics of light field manipulations, the spatial displacement of light beams at optical interfaces represents a fundamental wave phenomenon and an essential approach for light field manipulation.[29–31] When light encounters an optical interface, various beam displacement phenomena can arise, notably the spin Hall effect of light and the Goos-Hänchen shift.[32,33] These beam shifts reflect the intricate interactions between light's different degrees of freedom at interfaces, ranging from simple boundaries to complex photonic structures. They offer valuable insights into fundamental wave physics and have enabled diverse applications such as bio-sensing and precision metrology.[30,34,35] While conventional optical interfaces can naturally exhibit beam shifts, the typically small magnitudes and limited efficiencies of these shifts have driven research toward enhancing these effects using engineered photonic structures.[36–38] Recent advances in nanophotonic platforms, particularly in PhC slabs, have demonstrated various methods for achieving light beam displacements.[17,18,39–42] However, achieving controllable beam shifts that combine large displacement with high efficiency present substantial challenges and show fundamental importance in advancing optical technologies, as both parameters are critical yet difficult to optimize simultaneously. It is of vital significance to develop new approach for continuously tunable and efficient beam shift manipulation.

S. Wu, X. Wang, X. Zhao, L. Rao, W. Liu, J. Wang, L. Shi, J. Zi
State Key Laboratory of Surface Physics
Key Laboratory of Micro- and Nano-Photonic Structures (Ministry of Education) and Department of Physics
Fudan University
Shanghai 200433, China
E-mail: jiajunwang@fudan.edu.cn; lshi@fudan.edu.cn
W. Liu, L. Shi, J. Zi
Institute for Nanoelectronic Devices and Quantum Computing
Fudan University
Shanghai 200438, China
L. Shi, J. Zi
Collaborative Innovation Center of Advanced Microstructures
Nanjing University
Nanjing 210093, China
L. Shi, J. Zi
Shanghai Research Center for Quantum Sciense
Shanghai 201315, China

The ORCID identification number(s) for the author(s) of this article can be found under https://doi.org/10.1002/lpor.202500913

DOI: 10.1002/lpor.202500913

In this study, we propose and experimentally demonstrate a high-efficiency approach for tunable light beam displacement manipulation through polarization control in a reflective PhC slab. Guided by temporal coupled mode theory (TCMT), the reflective PhC slab design can effectively enhance cross-polarization efficiency by suppressing the transmission channel, enabling clear and direct observation for beam shifts without additional polarization analysis. Combined with the momentum-space geometric phase gradient engineered in PhC design that facilitates significant lateral displacement, we further achieve continuously controllable beam shifts through incident polarization modulation. Experimentally, we demonstrate a practical maximum cross-polarization efficiency exceeding 74% and fully characterize the polarization steering beam shifts, with the displacement range reaching up to 14 wavelengths at 780 nm. Moreover, we show that the beam shift remains highly tunable across a range of incident wavelengths, providing an extra degree of freedom for precise beam manipulation. Our results underscore the potential of high-efficiency PhC slabs as compact platforms for polarization-controlled beam steering, advancing the frontier of micro/nano photonic devices in light field engineering.

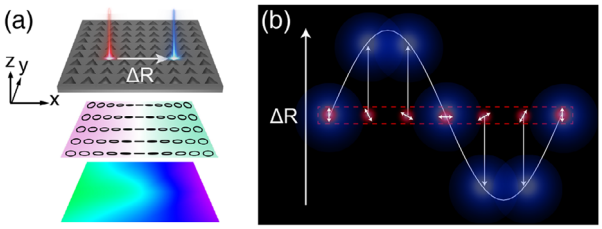

Figure 1. Schematic of polarization steering light beam shifts. a) Upper panel: A light beam (red) strikes a PhC slab consisting of a periodic dielectric structure on a flat metal surface, the reflected light (blue) experiences a shift, with the shift magnitude denoted as ΔR. Middle panel: The structure of polarization eigenstates near the center of the momentum space, with different colors representing varying elliptical polarizations (S_3/S_0). The mirror symmetry gives rise to eigen polarization with opposite chirality, which leads to an asymmetric phase distribution of the cross-polarized component in momentum space, thereby introducing a phase gradient. Lower panel: The phase distribution in momentum space for the cross-polarized components of the reflected light. b) The magnitudes of the beam shift vary for different linear polarization states of light when incident on the PhC slab. The incident beam is marked with red, with its polarization direction indicated by an arrow. The reflected beam is shown in blue, following a curve.

2. Principle

We start from the design principle of the high-efficiency reflective PhC slab. Considering that a monochromatic plane wave incident on a PhC slab. According to TCMT,[43] the reflected Jones vector E_{out} and the incoming Jones vector E_{in} can be connected using a scattering matrix S:

$$|E_{out}\rangle = S|E_{in}\rangle = \begin{pmatrix} r_{11} & r_{12}e^{i\theta} \\ r_{21}e^{-i\theta} & r_{22} \end{pmatrix} |E_{in}\rangle \quad (1)$$

where the matrix elements $r_{11}, r_{12}, r_{21}, r_{22}$ are reflection coefficients, and the subscripts 1 and 2 represent two orthogonal polarizations. Specifically, r_{11} and r_{22} denote the co-polarized reflection coefficients. The off-diagonal terms r_{12} and r_{21} represent the cross-polarized reflection coefficients, describing polarization conversion between the two basis states. These off-diagonal elements carry additional phase factors $e^{\pm i\theta}$, originating from the geometric phase.[15,17,44,45] For the PhC slab in **Figure 1a**, the mirror symmetry results in eigenpolarization modes with opposite chirality relative to the mirror plane.[8] This can lead to an inhomogeneous phase distribution $\varphi(k)$ in momentum space for the cross-polarized converted parts, as shown in the lower panel of Figure 1a. The phase gradient in momentum space causes a lateral shift of the beam in real space, with the relative shift given by[17,33,46]

$$\langle \Delta R \rangle = -\left\langle \frac{\partial \varphi(k)}{\partial k} \right\rangle \quad (2)$$

where $\langle \Delta R \rangle$ is the average shift in real space, and $\left\langle \frac{\partial \varphi(k)}{\partial k} \right\rangle$ is the average phase gradient in momentum space. For example, as shown in the upper panel of Figure 1a, when a linearly polarized Gaussian beam (red) is incident normally, the modulated reflected light (blue) undergoes a lateral shift of ΔR. This lateral shift is a direct consequence of the inhomogeneous phase distribution, which primarily arises from the geometric phase induced by cross-polarized conversion. Consequently, the cross-polarized components predominantly contribute to the beam shifts, while the co-polarized components with uniform momentum-space phase contribute little.

Therefore, the efficiency of reflective beam shift is dependent on the cross-polarized conversion efficiency. Low cross-polarized conversion diminishes the contribution from the geometric phase modulation, ultimately causing a less significant overall beam shift. In systems with low efficiency, polarization analysis is required to filter out the co-polarized components for a noticeable beam shift observation.[17,18] In contrast, high efficiency allows for the beam shift to be detected without the need for polarization analysis, enabling the obvious entire beam to shift. In typical systems, the presence of transmission and reflection channels often reduce cross-polarized efficiency. An effective method to increase efficiency is to turn off the transmission channel and focus solely on reflection.[16,47]

We consider a PhC slab with a single reflection channel, where a normally incident linearly polarized Gaussian beam has a polarization state $|\phi\rangle = \cos(\phi)\hat{x} + \sin(\phi)\hat{y}$, with ϕ representing the polarization angle. For an incident polarization state of $|\pm 45°\rangle = \frac{\sqrt{2}}{2}(\hat{x} \pm \hat{y})$, its conversion efficiency can be derived from the TCMT (see Section S2, Supporting Information, for details):

$$R_{cross}^{|\pm 45°\rangle} = \frac{\gamma_s^2}{(\gamma_0 + \gamma_s)^2 + (\omega - \omega_0)^2} \quad (3)$$

where ω_0 represents the eigenfrequency, ω is the source frequency, γ_0 is the intrinsic loss due to material absorption, and γ_s is the radiative loss. Theoretically, the conversion efficiency can reach 100% under resonant condition ($\omega = \omega_0$) when material absorption is absent ($\gamma_0 = 0$). Practically, high efficiency in reflective PhC slabs can still be realized

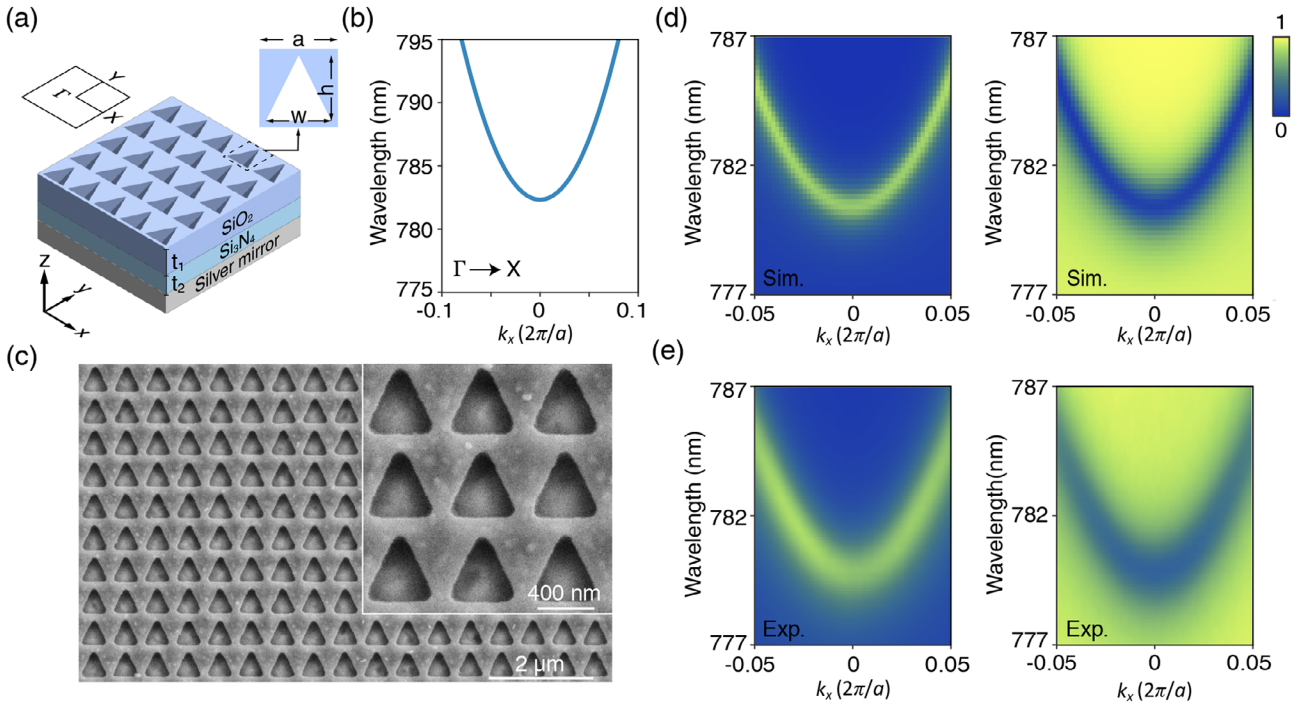

Figure 2. Design and optical characteristics of the photonic crystal slab. a) The photonic crystal slab is composed of three layers from top to bottom: silicon nitride (Si_3N_4), silica (SiO_2), and a silver mirror, with thicknesses t_1 and t_2 for the Si_3N_4 and SiO_2 layers, respectively. The triangular holes etched into the Si_3N_4 layer form a square lattice. The top-right inset shows a unit cell, featuring lattice constant a and hole height/width h/w. b) Simulated band structure along the Γ-X direction. c) Scanning electron microscopy (SEM) images of the fabricated sample. d,e) Simulated (d) and experimental (e) angle-resolved reflectance spectra under incident light in the polarization state $|+45°\rangle$, with left panels for cross-polarized and right panels for co-polarized analysis.

through mode selection and structural design that suppresses γ_0 while amplifying γ_s, overcoming the inevitable material absorption.[16]

For linearly polarized light incident on a lossless PhC slab, the conversion efficiency approaches 100% at the polarization states $|\pm45°\rangle$. At these two polarization states, the phase gradients are opposite, resulting in maximum beam shifts in opposite directions. Linearly polarized light at other polarization angles can be treated as a superposition of the two components at $|+45°\rangle$ and $|-45°\rangle$, leading to beam shifts that lie between the two extremes. For $|0°\rangle$ and $|+90°\rangle$ states, the contributions of the two components are equal, resulting in zero beam shift in both cases. Consequently, the beam shifts can be continuously tuned with the polarization angle, manifesting as the magnitude variation curve shown in Figure 1b. This reveals that polarization steering beam shifts can be achieved through a high-efficiency reflective PhC slab system.

3. Sample Design and Characterization

Following the design principles, the PhC slab consists of three layers from bottom to top: a silver mirror, a 100-nm-thick silica (SiO_2) layer, and a 130-nm-thick silicon nitride (Si_3N_4) layer. The unit cell is designed as a square lattice of triangular holes, with the lattice constant $a = 600$ nm and hole dimensions $w = h = 530$ nm, as illustrated in **Figure** 2a. The PhC structure without in-plane inversion symmetry is designed to engineer the geometric phase distribution in momentum space, as schematically shown in Figure 1a. Figure 2b presents the calculated band structures used for polarization steering beam shifts along the Γ-X direction. The far-field polarization eigenstates of the radiative modes on this band are simulated in Section S1 (Supporting Information), where the mirror-symmetric eigenpolarization states induce the momentum-space phase gradient along the Γ-X direction. Despite the absorption of the metal substrate, the reflective PhC slab maintains high efficiency, as shown in Figure 2d. The simulated angular-resolved reflectance spectra, with an incidence of $|+45°\rangle$ polarization state, demonstrate high cross-polarized conversion efficiency induced by PhC resonances (left panels, analyzed by $|-45°\rangle$ state) and low co-polarized efficiency (right panels, analyzed by $|+45°\rangle$ state).

Experimentally, the high-efficiency PhC slab was fabricated according to the design (see Experimental Section and Section S3, Supporting Information, for details on the fabrication process). The scanning electron microscopy (SEM) images in Figure 2c demonstrate that the fabricated sample closely matches the design parameters and exhibits good uniformity. We then employed a home-made Fourier-optics-based momentum-space imaging spectroscopy system to measure the angular-resolved reflectance spectra, as shown in Figure 2e. With corresponding polarization analysis, the measured spectra align well with the simulations, confirming high conversion efficiency. Based on the experimental spectra, we chose the target wavelength to be 780 nm, where the conversion efficiency near the Γ point is high, and proceeded to measure the phase distribution and conversion efficiency in momentum space.

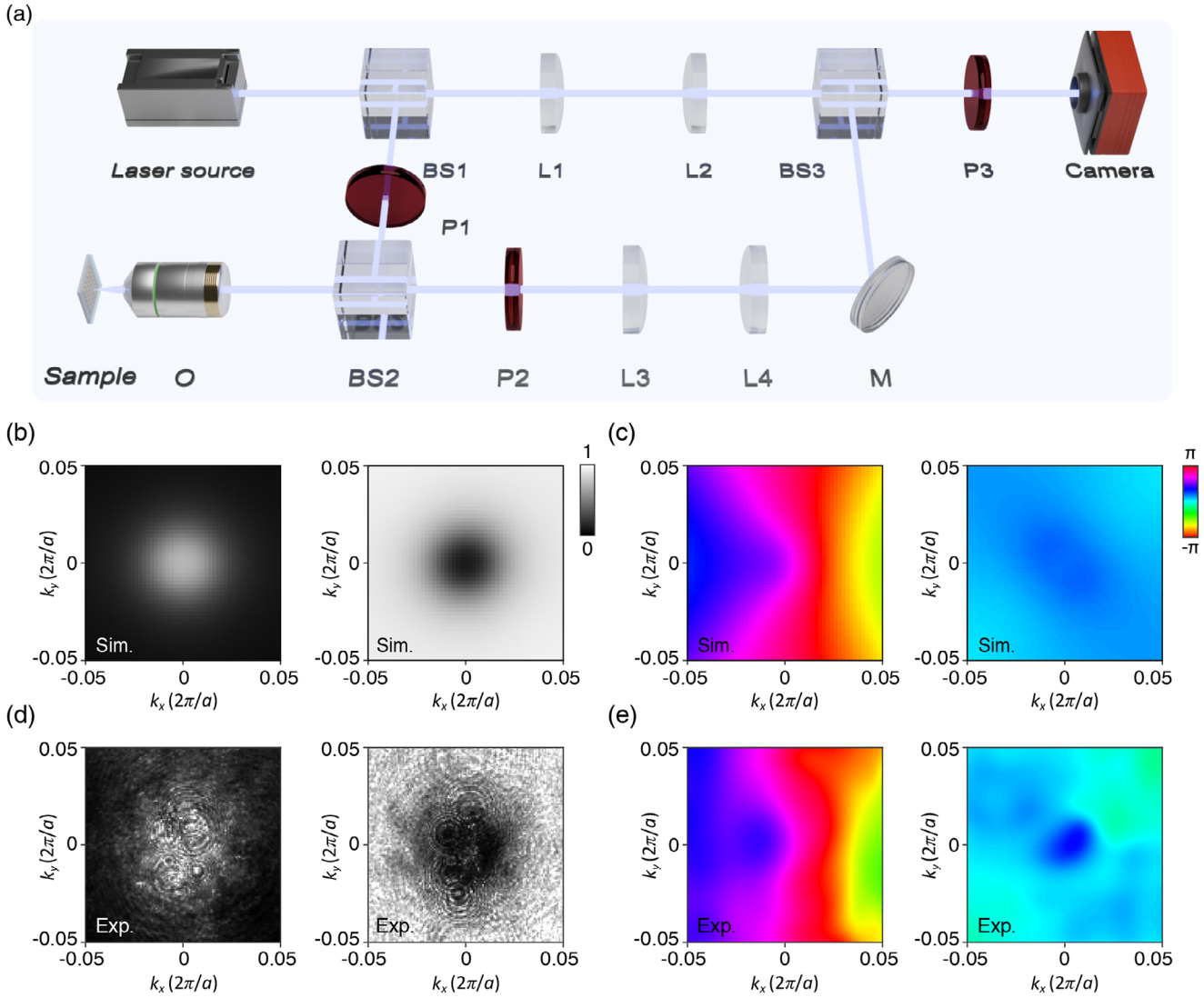

Figure 3. Experimental setup and polarization conversion characteristics of the sample. a) Off-axis interference-based momentum-space phase measurement system. BS, beam splitter; L, lens; P, polarizer; O, objective; M, mirror. After being split by the BS1, the beam is divided into a reference path and a sample path, and then recombined by the BS3. b,d) Cross-polarized (left panels) and co-polarized (right panels) conversion efficiency under incidence of the polarization state $|+45°\rangle$ at 780 nm, with simulation in (b) and experiment in (d). c,e) Phase distributions for cross-polarized (left panels) and co-polarized (right panels) processes at 780 nm, with simulation in (c) and experiment in (e).

To obtain these measurements, we employed an off-axis interference-based momentum-space phase measurement system,[15,16] as illustrated in **Figure 3**a. This setup can operate in two modes: an imaging mode and an interferometer mode, used for the precise measurements of conversion efficiency and phase distribution in momentum space, respectively.

In imaging mode, with no introduction of a reference beam and the final polarizer before the camera (P3) removed, the incident beam is polarized by a polarizer (P1) set to $|+45°\rangle$ polarization state and then focused by an objective lens (O). After passing through a second polarizer (P2), the reflected light is analyzed to measure the components of co-polarization or cross-polarization. The measured conversion efficiencies in momentum-space are shown in Figure 3d. The average cross-polarized conversion efficiency of regions around Γ point reaches nearly 70%, while the co-polarized efficiency is low, in good accordance with the simulated results (Figure 3b). Based on Equation (3), the efficiency can be improved through two approaches: reducing the intrinsic material loss γ_0 and enhancing the radiative loss. More discussions about conversion efficiency improvement are included in Section S10 (Supporting Information).

Subsequently, by introducing a reference beam and an additional polarizer (P3) to ensure both beams have the same polarization for interference, the system is switched to interferometer mode. Lens (L2) can introduce a slight angular tilt to the reference beam, and the phase information is then extracted from a single interferogram using a Fourier transform algorithm,[48] as presented in Figure 3e. In the cross-polarized case, there is a significant phase gradient along the k_x direction, while the phase gradient along the k_y direction is symmetric and averages out

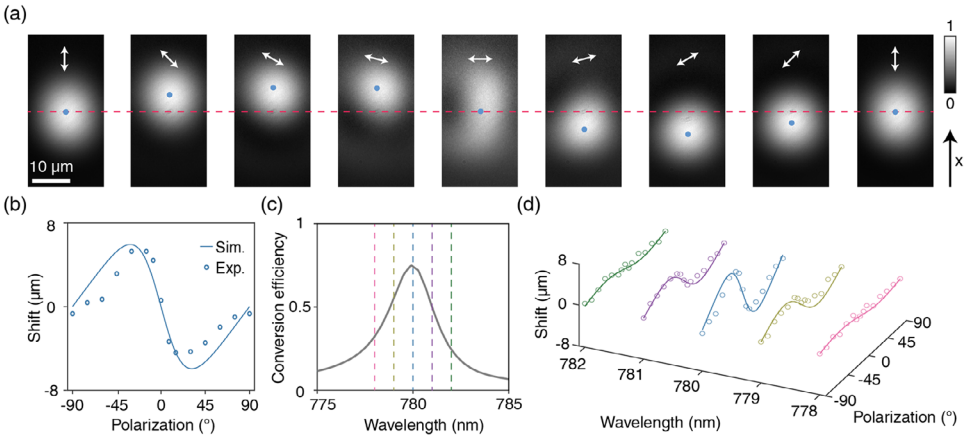

Figure 4. Experimentally observed polarization steering light beam shifts and beam shifts at different wavelengths. a) Positions and profiles of the reflected light beams at 780 nm under different linear polarization incidences. Blue dots mark the centroids of the beams, and arrows indicate the polarization angles of the incident light. b) Beam shifts under different linear polarization incidences at 780 nm. The solid line represents the simulated shifts and the dots represent the experimentally measured shifts. c) Cross-polarized conversion efficiency of reflected light at different wavelengths. The maximum conversion efficiency is achieved at an incident wavelength of 780 nm. d) Polarization-dependent beam shifts at different wavelengths. The solid lines represent the simulated shifts and the dots represent the experimentally measured shifts, with colors corresponding to (c).

to nearly zero. In contrast, the co-polarized case exhibits an almost negligible phase gradient, consistent with the simulation in Figure 3c, indicating that the co-polarized component has little influence on the beam shift. Furthermore, we also measured the phase distribution under incidence of $|-45°\rangle$ polarization state, as shown in Section S5 (Supporting Information), where the co-polarized case still exhibits almost zero phase gradient, while the cross-polarized phase gradient is reversed. With the high cross-polarized conversion efficiency, a pronounced polarization steering beam shift along the X direction for the reflective light can be directly observed without requiring polarization filtering, demonstrating the potential for polarization beam steering.

4. Polarization Steering Light Beam Shifts

The lateral beam shifts in real-space are directly observed using a reflective real-space imaging system (see Section S6, Supporting Information, for details). Only one polarizer is employed to control the polarization for incident light. **Figure** 4a clearly presents the profiles of the reflected light for incident polarization states varying from $|-90°\rangle$ to $|+90°\rangle$ at a wavelength of 780 nm, without polarization analysis. As the polarizer is rotated, the incident polarization state changes, resulting in both the profiles and the centroid of the reflected beam shifting simultaneously. The magnitude of the beam shift is defined by the difference in the centroid position of the reflected beam when incident on the PhC slab compared to that on unstructured region (indicated by the blue dots and red dashed line in Figure 4a, respectively). Figure 4b illustrates the polarization-dependent beam shifts along the X direction as a function of incident polarization.

For comparison, we simulated the momentum-space average phase gradient $\left\langle \frac{\partial\varphi(k)}{\partial k} \right\rangle$ of the reflected light for near-normal incidence with varying polarization states, which theoretically corresponds to the beam shift magnitude as described by Equation (2). The experimental dots and simulated curve show good agreement, with a tunable displacement range reaching up to 10.8 μm (≈14 wavelengths), demonstrating the realization of polarization steering light beam shifts via the high-efficiency PhC slab.

The high-efficiency reflective PhC slab also enables wavelength to serve as an additional degree of freedom for beam shifts. As shown in Figure 4c, the designed PhC slab exhibits significant variations in conversion efficiency with changing incident wavelengths, leading to notable differences in beam shifts. The cross-polarized conversion efficiency reaches a peak of nearly 74% at 780 nm, yielding the most pronounced beam shift at this wavelength. As the wavelength deviates from 780 nm, the decreasing conversion efficiency results in a corresponding reduction in the beam shift, as illustrated in Figure 4d. Notably, despite variations in beam shift magnitude at different wavelengths, polarization steering remains effective within a certain wavelength range. The reflected light beam profiles for different incident polarizations and wavelengths are provided in Section S7 (Supporting Information). These findings suggest that our designed high-efficiency PhC slab enables dual-parameter beam control through synergistic wavelength and polarization manipulation. This dual-dimensional control platform significantly enhances manipulation versatility while providing unprecedented flexibility in tailoring optical beam trajectories.

5. Discussion

In practice, the realization of beam shifts is subject to several limitations. One important limiting factor is the intrinsic material absorption, which directly affects the polarization conversion efficiency. In our experimental configuration, the dominant absorption arises from the silver layer. A detailed analysis of the impact of material absorption is provided in Section S9 (Supporting Information). As the absorption increases, the cross-polarized conversion efficiency decreases. Importantly, the polarization steering beam shift remains clearly observable. This robustness highlights the practical advantage of our approach, enabling effective beam manipulation under realistic material conditions and al-

lowing for further performance enhancement through material quality optimization.

In addition to material-related limitations, the divergence angle of the incident beam also affects the beam shift magnitude. A large divergence results in a broader momentum-space integration range, which reduces the averaged phase gradient and thus diminishes the beam shift, as shown in Section S9 (Supporting Information). Furthermore, the geometrical parameters of the PhC slab jointly determining the phase distribution and the beam shift. Section S11 (Supporting Information) analyzes polarization steering beam shifts under different values of a, w, and h, offering useful guidance for the design of future PhC slab structures.

Based on the existing results of beam shift studies and the practical limitations, there are some promising directions for future research. One important direction is to further enhance the efficiency of the polarization steering beam shift. This can be achieved by reducing material absorption, for example, by replacing silver with alternative low-loss materials, to improve cross-polarized conversion efficiency. In parallel, structural optimization of the PhC slabs, such as increasing the phase gradient or enhancing the γ_s values through tailored unit cell design, can effectively increase the average phase gradient and thus enlarge the resulting beam shift. Another promising avenue involves engineering the polarization field to realize in-plane average phase gradients that are not limited to the k_x direction. Such designs would enable steering of the output beam in arbitrary in-plane directions, paving the way for more versatile and functional photonic devices.

6. Conclusion

In conclusion, we have demonstrated a high-efficiency method for steering light beam shifts using a reflective PhC slab, leveraging polarization control to achieve tunable spatial displacements. By engineering the PhC structure to suppress transmission and enhance cross-polarized conversion, we achieved directly observable beam shifts without polarization filtering. Both theoretical and experimental results confirm continuously tunable displacements via incident polarization, reaching up to ≈14 wavelengths at 780 nm. Wavelength-dependent measurements further introduce a secondary tuning dimension, expanding the control flexibility. Future research focusing on low-loss materials and optimized PhC slab designs could further improve conversion efficiency and broaden the tunable beam shift range. The demonstrated polarization-steering mechanism holds strong potential for beam-steering photonic devices, where incident polarization may serve as an active tuning degree of freedom for compact and efficient direction control.

7. Experimental Section

Sample Fabrication: Section S3 (Supporting Information) illustrates the detailed fabrication process of the PhC slab sample, which is constructed on a silicon substrate. First, a 240-nm-thick silver layer was deposited on the silicon substrate by magnetron sputtering to form the mirror layer. Next, the SiO_2 layer (100 nm thick) and Si_3N_4 layer (130 nm thick) were sequentially grown by plasma-enhanced chemical vapor deposition (PECVD). For the patterning process, a 300-nm-thick positive electron-beam resist (CSAR 62) was spin-coated onto the Si_3N_4 layer, followed by the application of a conductive polymer layer (AR-PC 5092.02). The pattern was transferred from the resist mask to the Si_3N_4 layer through reactive ion etching (RIE) using a CHF_3/O_2 gas mixture with a flow ratio of 45/5, RF power of 125 W, chamber pressure of 150 mTorr, and an etching duration of 180 s. Finally, the residual resist mask was removed using O_2 plasma cleaning.

Numerical Simulations: The eigenmode simulations, conversion efficiency, and phase distribution in momentum-space were computed using a finite-element method, with periodic boundary conditions applied in the x and y directions and a second-order scattering boundary condition in the z direction.

Supporting Information

Supporting Information is available from the Wiley Online Library or from the author.

Acknowledgements

This work was supported by National Key R&D Program of China (Nos. 2023YFA1406900 and 2022YFA1404800); National Natural Science Foundation of China (Nos. 12234007, 12321161645, 12221004, T2394480, T2394481, 12404427, and 124B2084); Science and Technology Commission of Shanghai Municipality (22142200400, 21DZ1101500, 2019SHZDZX01, 23DZ2260100, 24YF2702400, and 24142200100). J.W. was further supported by China National Postdoctoral Program for Innovative Talents (BX20230079) and China Postdoctoral Science Foundation (2023M740721).

Conflict of Interest

The authors declare no conflict of interest.

Author Contributions

S.W., X.W., and X.Z. contributed equally to this work.

Data Availability Statement

The data that support the findings of this study are available from the corresponding author upon reasonable request.

Keywords

beam shift, high conversion efficiency, momentum-space polarization field, photonic crystal slab, polarization conversion

Received: April 17, 2025
Revised: August 22, 2025
Published online:

[1] A. F. Koenderink, A. Alù, A. Polman, *Science* **2015**, *348*, 516.

[2] A. I. Kuznetsov, A. E. Miroshnichenko, M. L. Brongersma, Y. S. Kivshar, B. Luk'yanchuk, *Science* **2016**, *354*, aag2472.
[3] H.-H. Hsiao, C. H. Chu, D. P. Tsai, *Small Methods* **2017**, *1*, 1600064.
[4] C. W. Hsu, B. Zhen, J. Lee, S.-L. Chua, S. G. Johnson, J. D. Joannopoulos, M. Soljačić, *Nature* **2013**, *499*, 188.
[5] B. Zhen, C. W. Hsu, L. Lu, A. D. Stone, M. Soljačić, *Phys. Rev. Lett.* **2014**, *113*, 257401.
[6] Y. Zhang, A. Chen, W. Liu, C. W. Hsu, B. Wang, F. Guan, X. Liu, L. Shi, L. Lu, J. Zi, *Phys. Rev. Lett.* **2018**, *120*, 186103.
[7] H. M. Doeleman, F. Monticone, W. den Hollander, A. Alù, A. F. Koenderink, *Nat. Photonics* **2018**, *12*, 397.
[8] W. Liu, B. Wang, Y. Zhang, J. Wang, M. Zhao, F. Guan, X. Liu, L. Shi, J. Zi, *Phys. Rev. Lett.* **2019**, *123*, 116104.
[9] T. Yoda, M. Notomi, *Phys. Rev. Lett.* **2020**, *125*, 053902.
[10] X. Wang, J. Wang, X. Zhao, L. Shi, J. Zi, *ACS Photonics* **2022**, *10*, 2316.
[11] C. W. Hsu, B. Zhen, A. D. Stone, J. D. Joannopoulos, M. Soljačić, *Nat. Rev. Mater.* **2016**, *1*, 1.
[12] M. Kang, T. Liu, C. Chan, M. Xiao, *Nat. Rev. Phys.* **2023**, *5*, 659.
[13] L. Huang, L. Xu, D. A. Powell, W. J. Padilla, A. E. Miroshnichenko, *Phys. Rep.* **2023**, *1008*, 1.
[14] J. Wang, P. Li, X. Zhao, Z. Qian, X. Wang, F. Wang, X. Zhou, D. Han, C. Peng, L. Shi, J. Zi, *Photon. Insights* **2024**, *3*, R01.
[15] B. Wang, W. Liu, M. Zhao, J. Wang, Y. Zhang, A. Chen, F. Guan, X. Liu, L. Shi, J. Zi, *Nat. Photonics* **2020**, *14*, 623.
[16] T. Li, J. Wang, W. Zhang, X. Wang, W. Liu, L. Shi, J. Zi, *Natl. Sci. Rev.* **2023**, *10*, nwac234.
[17] J. Wang, M. Zhao, W. Liu, F. Guan, X. Liu, L. Shi, C. T. Chan, J. Zi, *Nat. Commun.* **2021**, *12*, 6046.
[18] J. Wang, L. Shi, J. Zi, *Phys. Rev. Lett.* **2022**, *129*, 236101.
[19] J. Wang, H. Li, Y. Ma, M. Zhao, W. Liu, B. Wang, S. Wu, X. Liu, L. Shi, T. Jiang, J. Zi, *Light: Sci. Appl.* **2020**, *9*, 148.
[20] S. Kim, B. H. Woo, S.-C. An, Y. Lim, I. C. Seo, D.-S. Kim, S. Yoo, Q.-H. Park, Y. C. Jun, *Nano Lett.* **2021**, *21*, 10076.
[21] J. Tian, G. Adamo, H. Liu, M. Klein, S. Han, H. Liu, C. Soci, *Adv. Mater.* **2022**, *34*, 2109157.
[22] Y. Chen, H. Deng, X. Sha, W. Chen, R. Wang, Y.-H. Chen, D. Wu, J. Chu, Y. S. Kivshar, S. Xiao, C.-W. Qiu, *Nature* **2023**, *613*, 474.
[23] Y. Wang, D. Huang, M. Xia, J. Zhou, Y. Chen, Y. Liao, X. Zhang, *Adv. Mater.* **2024**, 2414174.
[24] C. Huang, C. Zhang, S. Xiao, Y. Wang, Y. Fan, Y. Liu, N. Zhang, G. Qu, H. Ji, J. Han, L. Ge, Y. Kivshar, Q. Song, *Science* **2020**, *367*, 1018.
[25] L. Carletti, K. Koshelev, C. De Angelis, Y. Kivshar, *Phys. Rev. Lett.* **2018**, *121*, 033903.
[26] Z. Liu, Y. Xu, Y. Lin, J. Xiang, T. Feng, Q. Cao, J. Li, S. Lan, J. Liu, *Phys. Rev. Lett.* **2019**, *123*, 253901.
[27] T. Shi, Z.-L. Deng, G. Geng, X. Zeng, Y. Zeng, G. Hu, A. Overvig, J. Li, C.-W. Qiu, A. Alù, Y. S. Kivshar, X. Li, *Nat. Commun.* **2022**, *13*, 4111.
[28] W. Liu, J. Wang, Y. Tang, X. Wang, X. Zhao, L. Shi, J. Zi, C. Chan, *Nano Lett.* **2024**, *24*, 943.
[29] K. Y. Bliokh, F. J. Rodríguez-Fortu no, F. Nori, A. V. Zayats, *Nat. Photonics* **2015**, *9*, 796.
[30] X. Ling, X. Zhou, K. Huang, Y. Liu, C.-W. Qiu, H. Luo, S. Wen, *Rep. Prog. Phys.* **2017**, *80*, 066401.
[31] M. Kim, Y. Yang, D. Lee, Y. Kim, H. Kim, J. Rho, *Laser Photonics Rev.* **2023**, *17*, 2200046.
[32] O. Hosten, P. Kwiat, *Science* **2008**, *319*, 787.
[33] K. Y. Bliokh, A. Aiello, *J. Opt.* **2013**, *15*, 014001.
[34] T. Zhu, Y. Lou, Y. Zhou, J. Zhang, J. Huang, Y. Li, H. Luo, S. Wen, S. Zhu, Q. Gong, M. Qiu, Z. Ruan, *Phys. Rev. Appl.* **2019**, *11*, 034043.
[35] S. Chen, X. Ling, W. Shu, H. Luo, S. Wen, *Phys. Rev. Appl.* **2020**, *13*, 014057.
[36] X. Yin, Z. Ye, J. Rho, Y. Wang, X. Zhang, *Science* **2013**, *339*, 1405.
[37] H. Dai, L. Yuan, C. Yin, Z. Cao, X. Chen, *Phys. Rev. Lett.* **2020**, *124*, 053902.
[38] W. Zhu, H. Zheng, Y. Zhong, J. Yu, Z. Chen, *Phys. Rev. Lett.* **2021**, *126*, 083901.
[39] F. Wu, J. Wu, Z. Guo, H. Jiang, Y. Sun, Y. Li, J. Ren, H. Chen, *Phys. Rev. Appl.* **2019**, *12*, 014028.
[40] M. Kim, D. Lee, Y. Yang, Y. Kim, J. Rho, *Nat. Commun.* **2022**, *13*, 2036.
[41] F. Wu, T. Liu, M. Luo, H. Li, S. Xiao, *Phys. Rev. B* **2024**, *109*, 125411.
[42] M. Wei, Y. Long, F. Wu, G.-G. Liu, B. Zhang, *Sci. Bull.* **2025**, *70*, 882.
[43] S. Fan, W. Suh, J. D. Joannopoulos, *J. Opt. Soc. Am. A* **2003**, *20*, 569.
[44] M. V. Berry, *J. Mod. Opt.* **1987**, *34*, 1401.
[45] Z. Bomzon, G. Biener, V. Kleiner, E. Hasman, *Opt. Lett.* **2002**, *27*, 1141.
[46] L.-G. Wang, S.-Y. Zhu, *Opt. Lett.* **2006**, *31*, 101.
[47] W. Liu, L. Shi, J. Zi, C. T. Chan, *Nanophotonics* **2021**, *10*, 4297.
[48] N. Carlon Zambon, P. St-Jean, M. Milićević, A. Lemaître, A. Harouri, L. Le Gratiet, O. Bleu, D. Solnyshkov, G. Malpuech, I. Sagnes, S. Ravets, A. Amo, J. Bloch, *Nat. Photonics* **2019**, *13*, 283.